Available online at www.sciencedirect.com
ScienceDirect
Ceramics International 38S (2012) S669–S672
CERAMICS INTERNATIONAL
www.elsevier.com/locate/ceramint

Effect of the nitrogen inducing agents on the corrosion behavior of the oxide coatings prepared by electrolytic plasma processing on the Al2021 alloy

Kai Wang, Sang Sik Byeon, Yeon Gil Jung, Bon Heun Koo *

School of Nano & Advanced Materials Engineering, Changwon National University, Changwon 641-773, Republic of Korea

Available online 27 May 2011

Abstract

The AlON–Al_2O_3 oxide coatings were prepared on the Al2021 alloy by the electrolytic plasma processing (EPP) method at room temperature in 15 min under a hybrid voltage with various nitrogen inducing agents. The nitrogen inducing effects were studied by X-ray diffractometer (XRD), scanning electron microscopy (SEM). The corrosion behavior was evaluated by electrochemical tests in a 3.5 wt% NaCl solution under static conditions by open circuit potential and potentiodynamic polarization. The results show that $NaNO_2$ is a suitable steady nitrogen inducing agent to prepare a uniform and dense AlON–Al_2O_3 coating on the Al2021 alloy to protect the substrate corrosion.

Keywords: A. Films; C. Corrosion; D. Al_2O_3; D. Nitrides; AlON

1. Introduction

Plasma electrolytic oxidation (PEO) has been studied widely for its high efficiency of fabricating ceramic coatings on light metals (Al, Mg, Ti, etc.) [1]. PEO ceramic coatings offer an attractive combination of wear resistance, corrosion resistance, mechanical strength, interfacial adhesion, and thermal properties [2–6]. The PEO produced ceramic coatings are yet limited in microhardness and anti-abrasion properties for only Al_2O_3 hardening phase in the ceramic coatings. Creatively, nitrogen inducing agents were added into the PEO system to form an AlON second phase. Therefore, the new compromised PEO reaction is called as electrolytic plasma processing (EPP) [7,8].

In the present work, the EPP process was carried out to produce ceramic coatings on the Al2021 alloy in phosphate alkaline electrolytes under an optimized hybrid voltage. The effects of the nitrogen inducing agents on the corrosion behavior of the oxide coatings were investigated by open circuit potential and potentiodynamic polarizations. The surface morphology, microstructures of the oxide coatings were also characterized and related to the corrosion behavior.

2. Experimental

The Al2021 column samples (Cu, 5.8–6.8 wt%; Mg, 1.2–1.8 wt%; Si, 0.5 wt%; Fe, 0.5 wt%, Zn, 0.1 wt%; Mn, 0.2–0.4 wt%; Ti, 0.15 wt% and Al, balance) with a size of D 30 mm × H 16 mm and a surface finish of Ra ≤ 0.1 μm were used as the substrates after polished by 0.1 μm diamond paste. An EPP coating unit designed and built by the authors has been employed in the present study, which mainly consists of a power supply unit, a bath container and a cooling system. The basic electrolysis environment was an aqueous electrolyte containing 10 g/l Na_3PO_4 and 2 g/l NaOH. The nitrogen inducing agents were added with 0.5 g/l $NaNO_2$, $NaNO_3$ and NH_4NO_3, respectively. The AC amplitude was slowly increased to 200 V and then the DC value was increased gradually with time till 260 V to obtain a steady current of 10 A. The treating time was calculated to 15 min. Samples were rinsed with distilled water after EPP procedures.

The different phases present in the coatings were investigated with Philips-X'Pert system X-ray diffractometer (XRD) (Cu Kα radiation) and the scans were performed with 0.02° θ step size in the 2θ range of 20–90°. The microstructure of surfaces and cross sections of samples by different nitrogen inducing agents were examined by a JSM 5610 scanning electron microscopy (SEM). Open circuit potential and

* Corresponding author. Tel.: +82 55 264 5431; fax: +82 55 262 6486.
E-mail address: bhkoo@changwon.ac.kr (B.H. Koo).

0272-8842/$36.00
doi:10.1016/j.ceramint.2011.05.132

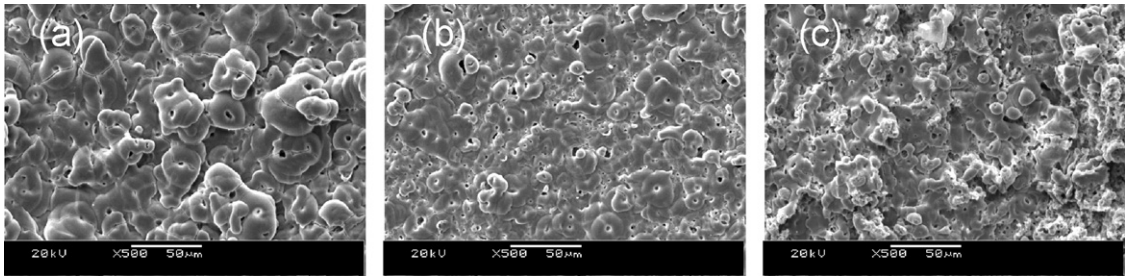

Fig. 1. SEM micrographs of the oxide coatings treated in (a) $NaNO_2$, (b) $NaNO_3$ and (c) NH_4NO_3 induced electrolytes.

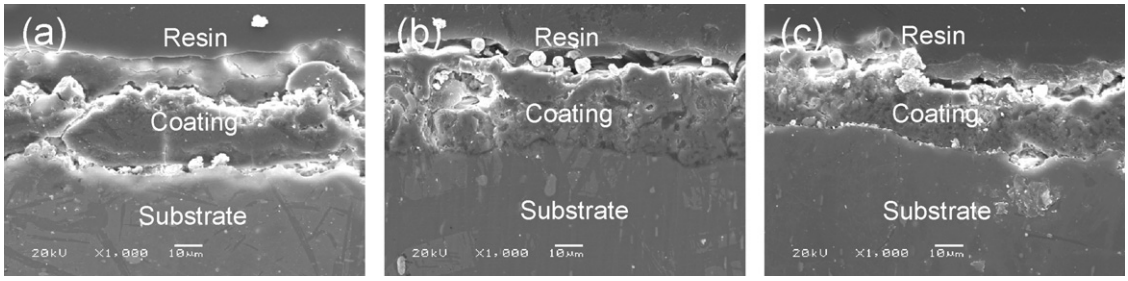

Fig. 2. Cross sections of the oxide coatings EPP treated in (a) $NaNO_2$, (b) $NaNO_3$ and (c) NH_4NO_3 induced electrolytes.

potentiodynamic polarization tests were performed by a Gamry Instrument (USA/CMS 1058). The test electrolyte consisted of a 3.5 wt% (0.6 M) NaCl solution at 20 °C. A saturated calomel electrode (SCE) was used as the reference electrode, and a graphite rod served as the counter electrode for current measurement. The potential was increased from −3.5 V_{SCE} to 4.5 V_{SCE} (vs. open circuit potential) with a scanning rate of 5 mV/s. All potentials are given with respect to the SCE. The working surface of each specimen was polished to a final finish with 1 μm diamond paste. The specimens were mounted in the electrochemical cell so that the surface area (1.1 cm^2) could be contacted with the test solution. The corrosion current density was determined by linear extrapolation of the polarization curves up to ±50 mV from the corrosion potential.

3. Results and discussion

Fig. 1 illustrates the surface features of the oxide coatings on the Al2021 alloys EPP-treated in different nitrogen inducing electrolytes. The center holes are the plasma discharge channels, which caused the pancake-like cavities on the surface. The molten alumina flew out of the discharge channels into the cool electrolytes, and then quickly solidificated to form the dark circles around the discharge channels. The same morphologies and phenomenon were also observed in Refs. [1,6]. Both the coatings present uniformly distributed pancake like cavities resulted by the plasma discharge channels in $NaNO_2$ and $NaNO_3$ induced electrolytes (Fig. 1(a) and (b)), while the pan-cake like structures shattered into pieces in the NH_4NO_3 induced electrolyte (Fig. 1(c)). It might be the reason that nitrogen from the NH_4^+ cation side would interrupt the solidification of the molten alumina. Therefore, the whole circle structure scattered into particles, and uniformly distributed around the discharge channels. The size of discharge channels are the largest of the $NaNO_2$ induced sample, as proved that inducing $NaNO_2$ is good for the growth of the oxide coatings.

The cross-sectional SEM images of coatings EPP-treated in various nitrogen inducing electrolytes are shown in Fig. 2. From Fig. 2(a), a dense oxide coating grew on the Al2021 alloy in the $NaNO_2$ induced electrolytes, as is benefit for the growth of the coatings. The oxide coatings turned to the porous structures while the EPP treatments were carried out in the $NaNO_3$ and induced NH_4NO_3 electrolytes (Fig. 2(b) and (c)). It can be concluded that the EPP reactions are stable to occur in the nitrite induced electrolytes compared to the reactions in the nitrate induced electrolytes, as the transformation of the nitrite to the nitrate could not be ignored. It was found by Koike and Hattori [9] that the reduction of nitrate to nitrite, nitrite to

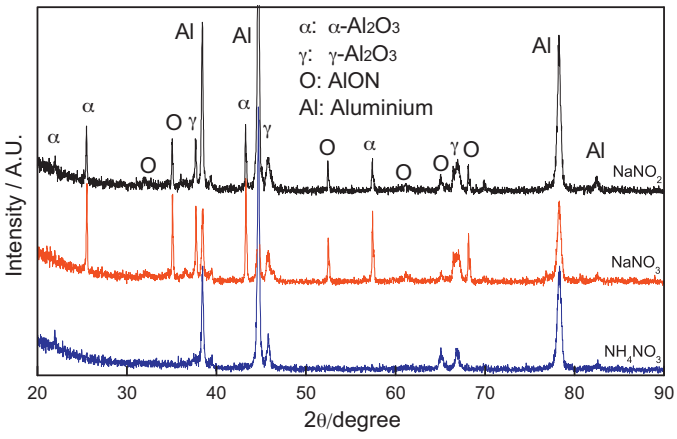

Fig. 3. XRD spectra of the oxide coatings on the Al2021 alloy in various nitrogen inducing electrolytes.

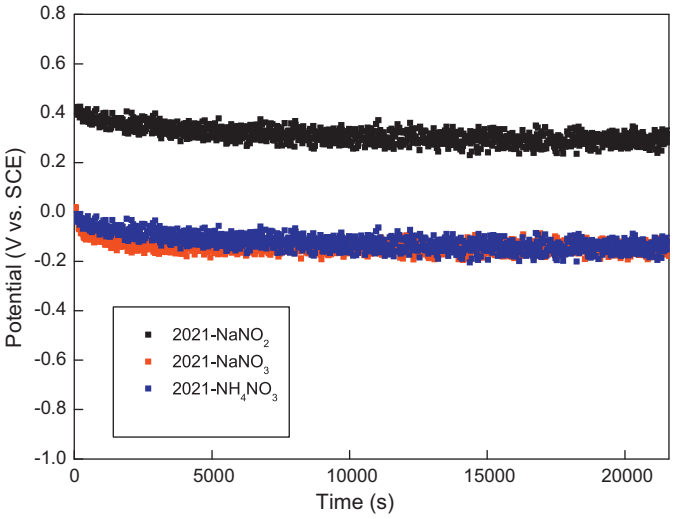

Fig. 4. Open circuit potential vs. exposure time of the oxide coatings treated in various nitrogen inducing electrolytes in a 3.5 wt% NaCl solution.

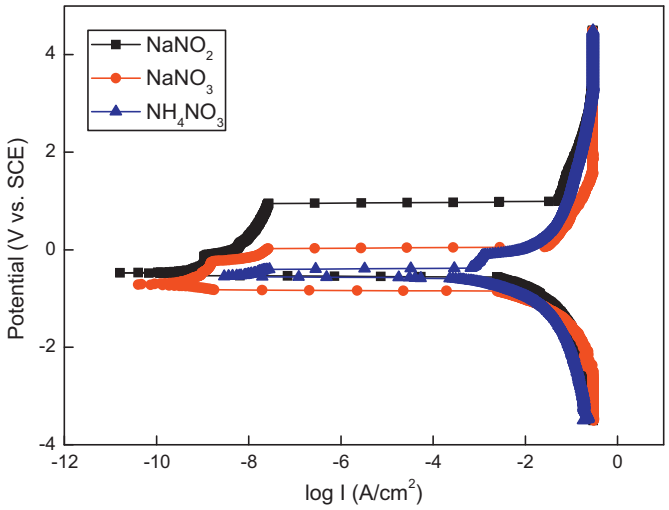

Fig. 5. Potentiodynamic polarization curves of the oxide coatings treated in various nitrogen inducing electrolytes in a 3.5 wt% NaCl solution.

nitrous oxide and nitrous oxide to nitrogen. Moreover, nitrogen from the NH_4^+ cation side would also aggravate the EPP reaction [10]. Because of the drastic plasma reactions in the electrolytes induced with NH_4^+ and NO_3^-, excess plasmas work for the molten of the alumina as to make it difficult to solidificate, which resulted in the formation of the porous oxide coatings. Hence, for the high bonding energy of $NaNO_2$ [9], a stable EPP reaction in $NaNO_2$ induced electrolyte resulted in a dense oxide layer.

The phase analysis of the oxide coatings by XRD on Al2021 alloys produced in different nitrogen inducing electrolytes is presented in Fig. 3. The typical phase composition of EPP coatings consists of α-Al_2O_3, γ-Al_2O_3 and AlON according to the XRD spectra of coatings EPP-treated in $NaNO_3$, $NaNO_2$ and NH_4NO_3 inducing electrolytes. From the XRD patterns, weak peaks of AlON and α-Al_2O_3 phases were found in the coatings prepared in $NaNO_3$ containing electrolyte, as indicated weak transformation of AlON and α-Al_2O_3 phases. While strong peaks of AlON and α-Al_2O_3 phases were detected in the coatings prepared in both $NaNO_2$ and NH_4NO_3 inducing electrolytes. Molten aluminum flew outwards through the discharging channels, as to oxide to form γ-Al_2O_3 [1,6]. With the participation of nitrogen from the electrolytes, then the γ-Al_2O_3 reacted with nitrogen to form AlON phase [11]. At the same time, γ-Al_2O_3 would transform to α-Al_2O_3 at a sharp temperature gradient. The formation of AlON and phase transformation of Al_2O_3 resulted in the growth of the layers when being ejected from the channels and rapidly quenched at the interface between electrolyte and substrates. More AlON phase formed in $NaNO_2$ induced electrolyte to form a dense oxide coating.

Fig. 4 shows the open circuit potential (OCP) vs. time curves for the oxide coatings on the Al2021 alloy in various nitrogen inducing electrolytes immersed in a 3.5 wt% NaCl solution. The amount of time taken to achieve the stabilization of the OCP is related to both the activation energy and the oxide coatings on the alloy surface. The exact time is dependent on the type of alloy and the electrolyte chemical composition. In this study, the OCP changes from the more negative potentials of the $NaNO_3$ and NH_4NO_3 induced samples to the more positive potentials of the $NaNO_2$ induced sample. A potential shift to a more anodic direction of $NaNO_2$ induced sample, whose value maintained at 0.29 V_{SCE}, as is associated with the formation of a dense protective passive oxide coating upon the alloy surface. While the potentials shift to cathode directions of $NaNO_3$ and NH_4NO_3 induced samples, whose values stayed around −0.14 V_{SCE}, as is due to that the NaCl corrosion solutions would easily penetrate through the porous coatings to reach the Al2021 alloy substrate.

Polarizations in both the cathodic and anodic directions were observed in the open circuit potential after 21,000 s during the OCP tests in a 3.5 wt% NaCl solution. The polarization curves of the tested samples were plotted in Fig. 5. The Tafel lines are characterized by the slope of the linear part of the polarization curve and by their intercept when extrapolated to the equilibrium potential. The intercept is proportional to the logarithm of the exchange current density, and the value of the current at their intersection is the rate of corrosion "i_{corr}" expressed in current density. The corrosion potentials, corrosion rates and anodic/cathodic Tafel slopes (β_A and β_C) are calculated from Fig. 5. The polarization resistance (R_p) values were determined by the following relationship [12,13]:

$$R_p = \frac{\beta_A \times \beta_C}{2.3 \times i_{corr}(\beta_A + \beta_C)} \quad (1)$$

where i_{corr} is the corrosion current density. This equation is based on the approximate linear polarization at the pitting corrosion potential (E_{pit}). A summary of the results of the potentiodynamic corrosion tests is given in Table 1.

The value of E_{pit} can reach to 0.9387 V_{SCE} in the $NaNO_2$ electrolyte and it decreased to 0.0245 V_{SCE} and −0.4011 V_{SCE}

Table 1
Corrosion potential and corrosion current density of the oxide coatings in various nitrogen electrolytes.

Nitrogen types	E_{pit} (V_{SCE})	I_{corr} ($\mu A/cm^2$)	Anodic Tafel slope β_A	Cathode Tafel slope β_C	R_p
$NaNO_2$	0.9387	0.0122	2.6813	0.6096	17.67
$NaNO_3$	0.0245	0.0274	2.2517	1.2911	12.98
NH_4NO_3	−0.4011	0.0244	3.9389	0.8322	12.19

in the $NaNO_3$ and NH_4NO_3 electrolytes, respectively. The corrosion current density of the coated Al alloys was lower than that of the aluminum alloy substrates. The EPP oxide coatings are difficult to passivate. The corrosion resistance of the samples EPP treated in the $NaNO_3$ and NH_4NO_3 electrolytes, decreased considerably because the corrosive solution would easily penetrate into porous protective oxide coatings, and reach the substrate. The results of polarization resistance show that the porous oxide coatings formed in the $NaNO_3$ and NH_4NO_3 electrolytes keeps at a same level around 12. As a dense oxide coating grew in the $NaNO_2$ electrolyte due to the formation of more AlON phase, the polarization resistance of $NaNO_2$ induced sample can achieve a higher value of 17.

4. Conclusions

The EPP treatments were carried out on the Al2021 alloy substrate in a solution of phosphate electrolytes with various nitrogen inducing agents in 15 min under a hybrid voltage (260 V DC and 200 V AC). The oxide coatings with pancake-like structures formed on the Al2021 alloy with the inducing of $NaNO_2$ and $NaNO_3$, and it began to scatter when induced with NH_4NO_3. The oxide coatings were consisted of AlON, γ-Al_2O_3 and α-Al_2O_3. $NaNO_2$ is proved to be the suitable steady nitrogen inducing agent to prepare a uniform and dense AlON–Al_2O_3 coating on the Al2021 alloy, which has good corrosion resistance to protect the substrate corrosion.

Acknowledgements

This reasearch was financially supported by the Ministry of Knowledge Economy (MKE-2009-T100200025). This research was supported by the MKE (The Ministry of Knowledge Economy), Korea, under the ITRC (Information Technology Research Center) support program supervised by the NIPA (National IT Industry Promotion Agency) (NIPA-2010-C1090-1021-0015).

References

[1] A.L. Yeronkhin, X. Nie, A. Leyland, A. Matthews, S.J. Dowey, Plasma electrolysis for surface engineering, Surface and Coatings Technology 122 (1999) 73–93.
[2] J.A. Curran, H. Kalkancı, Yu. Magurovaand, T.W. Clyne, Mullite-rich plasma electrolytic oxide coatings for thermal barrier applications, Surface and Coatings Technology 201 (2007) 8683–8687.
[3] S. Moon, Y. Jeong, Generation mechanism of microdischarges during plasma electrolytic oxidation of Al in aqueous solutions, Corrosion Science 51 (2009) 1506–1512.
[4] W.-C. Gu, G.-H. Lv, H. Chen, G.-L. Chen, W.-R. Feng, S.-Z. Yang, Characterisation of ceramic coatings produced by plasma electrolytic oxidation of aluminium alloy, Material Science Engineering A 447 (2007) 158–162.
[5] G. Lv, W. Gu, H. Chen, W. Feng, M.L. Khosa, L. Li, E. Niu, G. Zhang, S.-Z. Yang, Characteristic of ceramic coatings on aluminium by plasma electrolytic oxidation in silicate and phosphate electrolyte, Applied Surface Science 253 (2006) 2947–2952.
[6] A.L. Yerokhin, A.A. Voevodin, V.V. Lyubimov, J. Zabinsk, M. Donley, Plasma electrolytic fabrication of oxide ceramic surface layers for tribotechnical purposes on aluminium alloys, Surface and Coatings Technology 110 (1998) 140–146.
[7] K. Wang, S.S. Byeon, Y.J. Seo, C.G. Lee, B.H. Koo, Nitrogen inducing effect on preparation of AlON–Al_2O_3 coatings on Al6061 alloy by electrolytic plasma processing, Surface and Coatings Technology 205 (2010) S11–S14.
[8] S.S. Byeon, K. Wang, Y.G. Jung, B.H. Koo, Characteristic of AlON–Al_2O_3 coatings on Al6061 alloy by electrolytic plasma processing in aluminate and nitride electrolytes, Surface and Coatings Technology 204 (2010) 3196–3199.
[9] I. Koike, A. Hattori, Energy yield of denitrification: an estimate from growth yield in continuous cultures of pseudomonas denitrificans under nitrate-, nitrite- and nitrous oxide-limited conditions, Journal of General Microbiology 88 (1975) 11–19.
[10] L.P. Hadjipetrou, A.H. Stouthamer, Energy production during nitrate respiration by Aerobacter aerogenes, Journal of General Microbiology 38 (1965) 29–34.
[11] P. Tabary, C. Servant, J.A. Alary, Microstructure and phase transformations in the AlN–Al_2O_3 pseudo-binary system, Journal of the European Ceramic Society 20 (2000) 913–926.
[12] E. Poorqasemi, O. Abootalebi, M. Peikari, F. Haqdar, Investigating accuracy of the Tafel extrapolation method in HCl solutions, Corrosion Science 51 (2009) 1043–1054.
[13] G. Rocchini, Some considerations on the polarization resistance method, Corrosion Science 41 (1999) 2353–2367.